

CORE CREATION IN GALAXIES AND HALOES VIA SINKING MASSIVE OBJECTS

TOBIAS GOERDT^{1*}, BEN MOORE², J. I. READ^{3,2} AND JOACHIM STADEL²

¹Racah Institute of Physics, The Hebrew University, Jerusalem 91904, Israel

²Institut für Theoretische Physik, Universität Zürich, Winterthurerstrasse 190, CH-8057 Zürich, Schweiz

³Department of Physics & Astronomy, University of Leicester, University Road, Leicester, LE1 7RH, UK

Draft version December 4, 2018

ABSTRACT

We perform a detailed investigation into the disruption of central cusps via the transfer of energy from sinking massive objects. Constant density inner regions form at the radius where the enclosed mass approximately matches the mass of the infalling body. We explore parameter space using numerical simulations and give an empirical relation for the size of the resulting core within structures that have different initial cusp slopes. We find that infalling bodies always stall at the edge of these newly formed cores, experiencing no dynamical friction over many dynamical times. As applications, we consider the resulting decrease in the dark matter annihilation flux due to centrally destroyed cusps, and we present a new theory for the formation of close binary nuclei – the ‘stalled binary’ model. We focus on one particularly interesting binary nucleus system, the dwarf spheroidal galaxy VCC 128 which is dark matter dominated at all radii. We show that its nuclei would rapidly coalesce within a few million years if it has a central dark matter cusp slope steeper than r^{-1} . However, if its initial dark matter cusp is slightly shallower than a log slope of -0.75 at $\sim 0.1\%$ of the virial radius, then the sinking nuclei naturally create a core equal to their observed separation and stall. This is close to the log slope measured a recent billion particle CDM halo simulation.

Subject headings: cosmology: theory – dark matter – galaxies: dwarf – galaxies: individual: VCC 128 – methods: numerical

1. INTRODUCTION

Massive objects orbiting within a cuspy mass distribution are expected to lose momentum and sink via dynamical friction (Chandrasekhar 1943; White 1983; Hernquist & Weinberg 1989; Capuzzo-Dolcetta & Vicari 2005). While spiralling inwards the massive perturber transfers momentum to central particles/stars etc, moving them to a larger orbital radius. One effect of this process is to make an initially cuspy dark matter distribution shallower (El-Zant, Shlosman & Hoffman 2001; El-Zant et al. 2004; Tonini, Lapi & Salucci 2006; Ma & Boylan-Kolchin 2004; Jardel & Sellwood 2009).

In the prevailing Λ CDM cosmology, dark matter haloes are cuspy, having an inner density slope $\rho(r) \propto r^{-\gamma}$ with $\gamma > 1$ beyond $\approx 1\%$ of the virial radius (e.g. Dubinski & Carlberg 1991; Navarro 1996a; Diemand, Moore & Stadel 2005). By contrast, observations of dwarf galaxies seem to indicate that they have a cored mass distribution (e.g. de Blok, McGaugh & Rubin 2001; Sánchez-Salcedo, Reyes-Iturbide & Hernandez 2006; Kleyna et al. 2003), while controversial evidence for cored mass distributions in dwarf spiral galaxies has been debated for over a decade (Moore 1994).

Previously published work has demonstrated numerically (El-Zant, Shlosman & Hoffman 2001; El-Zant et al. 2004; Romano-Díaz et al. 2008; Ma & Boylan-Kolchin 2004; Merritt et al. 2004; Read et al. 2006a; Jardel & Sellwood 2009) and semi-analytically (Tonini, Lapi & Salucci 2006) that a sinking massive compact object – a *perturber* – will transfer energy and angular momentum to the background via

dynamical friction, creating a central constant density core from an initially cuspy density distribution. Once a core has formed, dynamical friction is no longer effective (Goerdt et al. 2006; Read et al. 2006a; Inoue 2009). Dynamical arguments show that sinking perturbers will stall at the outer edge of a core (Read et al. 2006a; Inoue 2009, 2010).

Here we quantify this stalling behaviour as a function of perturber mass M_{pert} and central cusp slope γ . We consider a much larger range in M_{pert} and γ than in previous papers (Goerdt et al. 2006; Read et al. 2006a) and find that stalling persists even at very high perturber mass, as found also recently by Gualandris & Merritt (2008). We also investigate how the cusp is physically transformed into a core.

The core formation mechanism we study is just one of several ways in which central cores can be formed. Core formation can also proceed by three-body encounters with a supermassive black hole binary (Milosavljević et al. 2002), as a result of rapid mass loss due to supernovae outflows (e.g. Navarro 1996b; Read & Gilmore 2005), or as a result of the rapid ejection of a central supermassive black hole due to anisotropic gravitational radiation recoil (e.g. Boylan-Kolchin et al. 2004). If these mechanisms play an important role then our derived stalling radii as a function of M_{pert} and γ will be lower bounds.

We consider two applications of our results. The first is the effect of cusp-destruction on the expected dark matter annihilation signal from galaxies and dwarf galaxies. For a wide range of popular dark matter particle models, dark matter can self-annihilate to produce γ -rays (Gunn et al. 1978). Since the signal goes as the dark matter density squared it is sensitive to the

* tobias.goerdt@uam.es

central density distribution (Silk & Bloemen 1987; Lake 1990). For our second application, we present a new theory for the formation of close binary nuclei – the ‘stalled binary’ model. Close binary nuclei with projected separation < 100 pc have been observed on a range of scales in the Universe (e.g. Lauer et al. 1993, 1996, 2005; Bender et al. 2005; Houghton et al. 2006; Mast et al. 2006; Debattista et al. 2006). The standard model for these has become the Tremaine (1995) eccentric disc model originally proposed to explain M31 (Lauer et al. 2005). However, when the double nucleus of M31 was first discovered, Lauer et al. (1993) speculated that the two bright nuclei really were just that – one from M31 and the other the cannibalised centre of a smaller merged galaxy. The primary argument against this was that dynamical friction would cause the nuclei to rapidly coalesce. We show that, as binary nuclei sink via dynamical friction, they create a central constant density core. They then stall at the edge of this core experiencing no further friction over many dynamical times. We apply our new ‘stalled binary’ model to one particularly interesting binary nucleus system – the dwarf spheroidal galaxy VCC 128 discovered by Debattista et al. (2006). We show that this galaxy is dark matter dominated at all radii. As a result – if its binary nucleus is a ‘stalled binary’ – VCC 128 gives us a unique opportunity to constrain the central log-slope of the dark matter density profile on very small scales.

This paper is organised as follows: In §2 we describe our analytical framework, which is supported using N -body simulations. In §3 we apply our findings to dark matter annihilation, to binary nuclei, and to the special case of VCC 128. Finally, in §4 we present our conclusions.

2. TRANSFORMING CUSPS TO CORES

2.1. Numerical models

We use the split-power law α, β, γ model for our initial background distribution (Hernquist 1990; Saha 1992; Zhao 1996):

$$\rho(r) = \frac{\rho_0}{(r/r_s)^\gamma [1 + (r/r_s)^\alpha]^{(\beta-\gamma)/\alpha}} \quad (r \leq R_{\text{vir}}) \quad (1)$$

where ρ_0 and r_s are the normalisation of the density and scale length respectively, γ is the inner log slope, β is the outer log slope, whereas α controls the transition between the inner and the outer region. Since we focus on the very inner regions of the halo in our analysis, α and β are not critical. We fix $\alpha = 1$ and $\beta = 3$ – the commonly accepted values for cold dark matter haloes. We explore a range of values for the central cusp slope γ .

We will take our fiducial model to represent a low mass dark matter halo typical of those surrounding dwarf galaxies with a maximum circular velocity $v_{\text{peak}} = 50$ km s⁻¹. As our application later, we will consider the Virgo cluster dwarf galaxy VCC 128 which has an absolute bolometric luminosity of $M_B = -15.5$ mag (Debattista et al. 2006). We estimate its maximum circular velocity to be $v_{\text{peak}} = 35 - 65$ km s⁻¹ using the Faber-Jackson relation of dEs (de Rijcke et al. 2005). We adopt a concentration parameter of 15 for $\gamma = 1.0$, which is a typical value found for cosmologically mo-

<i>Halo</i>	γ	$\rho_0 / \text{M}_\odot \text{pc}^{-3}$	r_s / kpc	con	$M_{\text{vir}} / \text{M}_\odot$
A	1.75	0.000232	20.8	3.88	3.10×10^{10}
B	1.50	0.001333	10.3	7.50	2.71×10^{10}
C	1.25	0.004029	6.59	11.5	2.57×10^{10}
D	1.00	0.009109	5.01	15.0	2.50×10^{10}
E	0.75	0.017732	3.91	19.0	2.43×10^{10}
F	0.50	0.027746	3.38	22.0	2.40×10^{10}

TABLE 1
PARAMETERS FOR THE SIX DIFFERENT DARK MATTER HALOES WE USE IN OUR ANALYTICAL AND NUMERICAL CALCULATIONS.

tivated dwarf spheroidals (Lokas 2002). This gives a $r(v_{\text{peak}})$ of 10.75 kpc. For our other models we keep v_{peak} as well as $r(v_{\text{peak}})$ constant and only vary γ . This leads to the parameters given in Table 1 and to the circular velocity curves and radial density profiles, which are shown in Figure 1.

The dynamical friction sinking timescale of a perturber in such a system can be derived using the Chandrasekhar dynamical friction formula (Chandrasekhar 1943). Assuming that the perturber is always on a circular orbit, and that the background particles have a Maxwellian velocity distribution, we can calculate the infall rate:

$$\frac{dr}{dt} = -\frac{4\pi \ln \Lambda(r) \rho(r) G^2 M_{\text{pert}} r}{v_c^2(r) d[r v_c(r)]/dr} \left\{ \text{erf} \left[\frac{v_c(r)}{\sqrt{2}\sigma(r)} \right] - \frac{2v_c(r)}{\sqrt{2\pi}\sigma(r)} \exp \left[\frac{-v_c^2(r)}{2\sigma^2(r)} \right] \right\}, \quad (2)$$

where $v_c(r)$ is the circular speed at radius r ; M_{pert} is the mass of the in-falling body; $\ln \Lambda(r)$ is the Coulomb logarithm [$\Lambda = b_{\text{max}}/b_{\text{min}}$]; $\rho(r)$ is the density of the dark matter halo at radius r according to equation (1); and $\sigma(r)$ is the one-dimensional velocity dispersion of the halo.

Equation (2) assumes that dynamical friction is a local process that proceeds by momentum exchange between the perturber and the background. This cannot be the whole story. Firstly, it implies that if $\rho(r) \rightarrow 0$ there will be no dynamical friction. Secondly, it implies that if $\rho(r) \rightarrow \text{const}$, nothing special should happen and dynamical friction should proceed as for any other $\rho(r)$. Both of these statements conflict with numerical results (Lin & Tremaine 1983; Tremaine & Weinberg 1984; Colpi, Mayer & Governato 1999; Goerdt et al. 2006; Read et al. 2006a). The implication is that dynamical friction is not only a local process, but also depends on global resonances (Tremaine & Weinberg 1984; Sellwood 2006; Read et al. 2006a). In the former case, resonances (and therefore friction) are present even outside of a galaxy where $\rho(r) = 0$. In the latter case, $\rho = \text{const}$ is a harmonic potential which is especially resonant. After a period of enhanced friction, the perturber and the background reach a stable state with no net momentum exchange (Kalnajs 1972; Read et al. 2006a). Despite the above difficulties, in most situations, equation (2) works remarkably well.

2.2. Results from N -body simulations

We now study the response of different central cusps to sinking perturbers with a range of masses using N -body simulations. We consider all of our haloes A –

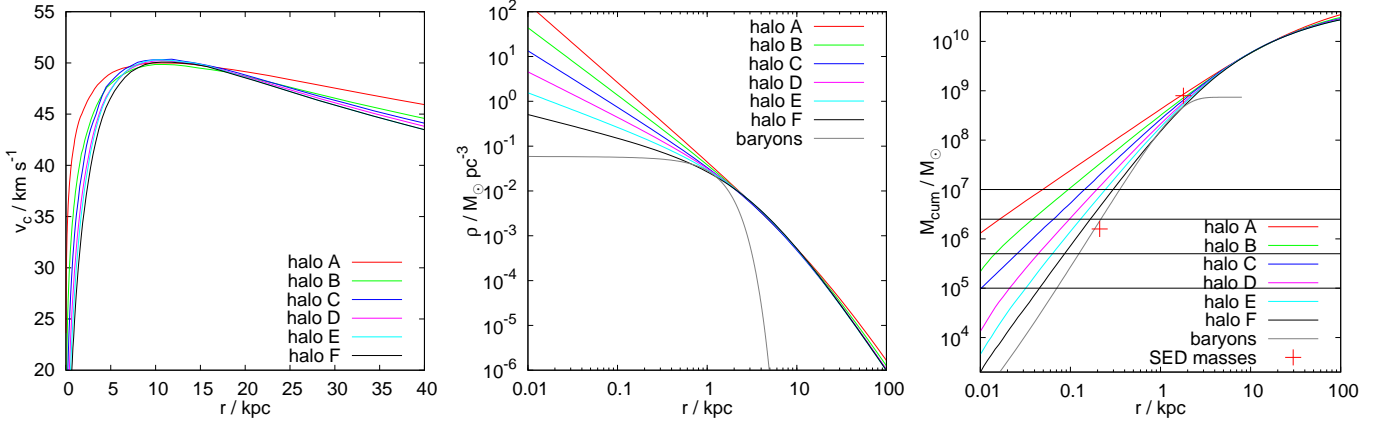


FIG. 1.— Circular velocities (*left*) radial density profiles (*middle*) and cumulative mass (*right*) for all our haloes A – F. These are constructed to have peak values of 50 km s^{-1} at 10.75 kpc . The horizontal black lines on the right panel show the perturber masses M_{pert} we use in the simulations (§2.2). The grey lines and the red crosses show estimates of the baryonic (stellar) mass distribution of the dSph galaxy VCC 128. Notice that in all models, VCC 128 is dark matter dominated at all radii.

F presented in Table 1. Equilibrium N -body representations of these haloes were created with the algorithm described in Kazantzidis, Magorrian & Moore (2004) using the multimass technique of Zemp et al. (2008). This gives structures that have an effective resolution in the region of interest equivalent to using $\sim 10^{10}$ single mass particles. The softening of the lightest particles is 0.1 pc . We ran a grid of simulations with $M_{\text{pert}} = [10^5, 5 \times 10^5, 2.5 \times 10^6, 10^7, 5 \times 10^7] M_{\odot}$ for each of the haloes A, B, C, D, E, F corresponding to varying the initial central log density slope: $\gamma = [1.75, 1.5, 1.25, 1, 0.75, 0.5]$ (see Table 1). The perturbers have softening lengths of 2 pc and were started at a radius of 0.4 kpc (within the cusp region), except for the heaviest perturbers which we had to start further out for reasons which will be explained in §2.2.1. (We could have started all nuclei at the outermost radius and obtained the same results, but this would have produced avoidable computational costs. See Figure 8.) All simulations are shown using circular orbits but similar scaling laws were found using more eccentric orbits.

It is well known that if you pick the wrong centre, a cuspy profile will appear to have a core (Beers & Tonry 1986). We used the particle with the lowest potential as the centre of the halo. In order to have a robust determination of the centre, we removed the perturber and only used the lightest halo particles. In addition, we double-checked our results against the ‘shrinking spheres method’ (e.g. Power et al. 2003; Goerdts et al. 2006; Read et al. 2006b). The results agreed up to the noise level. The resulting trajectories are given in Figure 2.

In order to double check the validity of modelling the perturber as just one single particle, we ran an additional simulation with a live ‘globular cluster’ as perturber. The live globular cluster we use consists of 10^5 particles which are distributed according to the King model (King 1966; Michie 1963; Michie & Bodenheimer 1963) given by

$$\rho(\Psi) = \rho_1 \exp\left(\frac{\Psi}{\sigma^2}\right) \text{erf}\left(\frac{\sqrt{\Psi}}{\sigma}\right)$$

$$- \rho_1 \sqrt{\frac{4\Psi}{\pi\sigma^2}} \left(1 + \frac{2\Psi}{3\sigma^2}\right), \quad (3)$$

where σ is the velocity dispersion, ρ is the density and Ψ is the relative potential. Each globular cluster is constructed with a $W_0 = \Psi(0)/\sigma^2$ parameter of 6, a total mass of $4.2 \times 10^5 M_{\odot}$, and a central velocity dispersion of 11 km/s . We use 0.05 pc for the gravitational softening lengths of its particles. This perturber is put into halo D at an initial distance of 0.4 kpc . Its trajectory can be seen in Figure 3. As one can clearly see the behaviour of the live perturber matches the behaviour of the single particle in this figure as well as in Figure 2 very well.

2.2.1. Cusp destruction, core creation and stalling

For all trajectories there is an apparent “kickback” which occurs after a first point of closest approach (fpca). The perturber seems to move away for a while, reaches a maximum, and then returns to a second point of closest approach (spca), where it finally stalls. For especially pronounced kickbacks, fpca and spca are marked by black crosses in Figure 2. This apparent “kickback” occurs at a point where the acceleration on the perturber due to the background is equal to the acceleration on the background due to the perturber, and the centre of mass of the system is significantly displaced. At this point the true ‘centre’ of the system becomes poorly defined. For this reason, the “kickback” feature is not physical but rather an artifact of our centring algorithm. After the “kickback”, the background rapidly rearranges itself to form a central constant density core, at which point the perturber stalls.

The density profiles of the respective host halo at fpca and at spca are plotted in Figure 4. One can clearly see that the density distribution changes significantly from cuspy to having a core: larger perturber masses lead to larger constant density central regions. The orange crosses in Figure 4 mark the ‘stalling radii’ where the perturber no longer sinks via dynamical friction. Notice that these lie at the edge of the freshly created core. For this reason, from here on we define the core radius to be the radius where the perturber stalls: $r_{\text{core}} = r_{\text{stall}}$.

2.2.2. Why do cusps become cores?

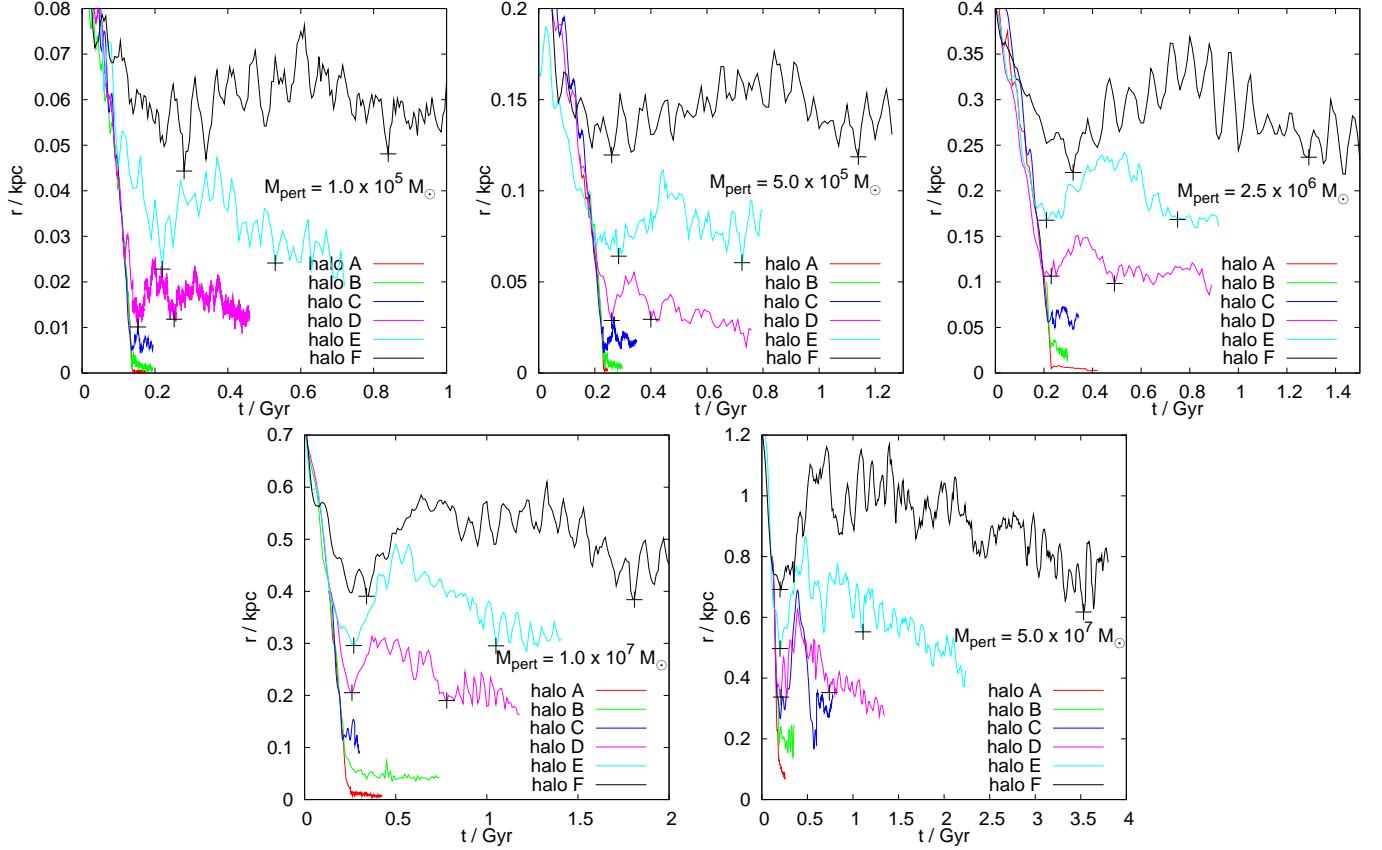


FIG. 2.— Simulated position of a single perturber within different haloes. From left to right the upper panels show perturber mass $M_{\text{pert}} = [10^5, 5 \times 10^5, 2.5 \times 10^6] M_{\odot}$ and the lower panels mass $M_{\text{pert}} = [10^7, 5 \times 10^7] M_{\odot}$. The black crosses indicate the first point of closest approach (fpca) and the second point of closest approach (spca).

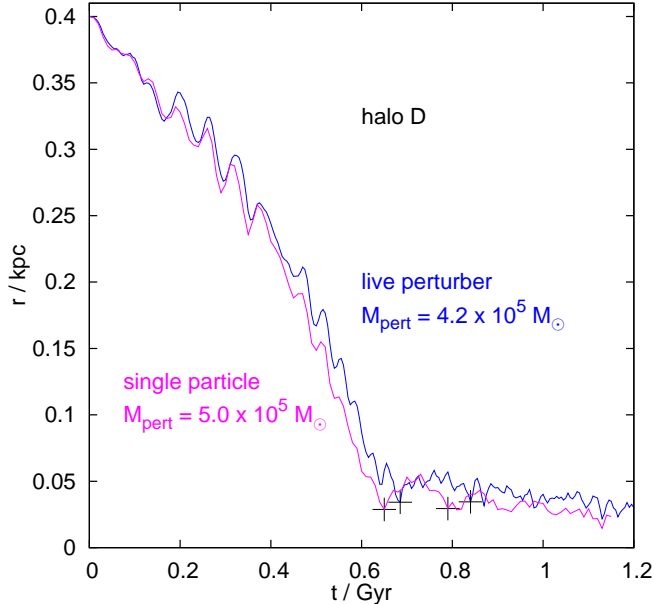


FIG. 3.— Simulated position of a live perturber of mass $M_{\text{pert}} = 4.2 \times 10^5 M_{\odot}$ compared to a single particle perturber of mass $M_{\text{pert}} = 5.0 \times 10^5 M_{\odot}$ both within halo D. The black crosses indicate the respective first point of closest approach (fpca) and second point of closest approach (spca).

Figure 5 shows $194 \text{ pc} \times 194 \text{ pc}$ density contour maps of background particles within halo C. We select only particles whose orbit lies within the plane of the perturber. The perturber mass was $5 \times 10^5 M_{\odot}$ and orbits *anticlockwise* on this figure (see red crosses). The different panels show output times: 185 Myr, 210 Myr, 235 Myr (the time of the fpca), 260 Myr, 285 Myr, 310 Myr and 335 Myr. The graph in the lower right corner shows the trajectory from Figure 2. The arrows indicate the above output times and the crosses mark the first and second points of closest approach (fpca and spca).

Notice that the cusp in halo C becomes tidally torn into an arc at $\sim 235 \text{ Myr}$. This suggests that tidal shredding of the cusp by the perturber is responsible for the cusp-core transformation. If true, then we would expect cusp-core transformations to occur at approximately the tidal radius r_t . This is where the mean density of the perturber roughly matches the mean density of the background $\bar{\rho}_{\text{pert}}(r_t) \sim \bar{\rho}_{\text{back}}(r_t)$, or equivalently where the mass of the perturber roughly matches the enclosed mass of the background $M_{\text{pert}} \sim M_{\text{back}}(r_t)$ (Read et al. 2006b).

Figure 6 shows the core radius r_{core} as a function of the radius which encloses the mass of the perturber in the initial conditions. We find a near-linear correlation, as expected from the above hypothesis. More concretely, we can write:

$$M_{\text{pert}} \sim M_{\text{back}}(r_t) \quad (4)$$

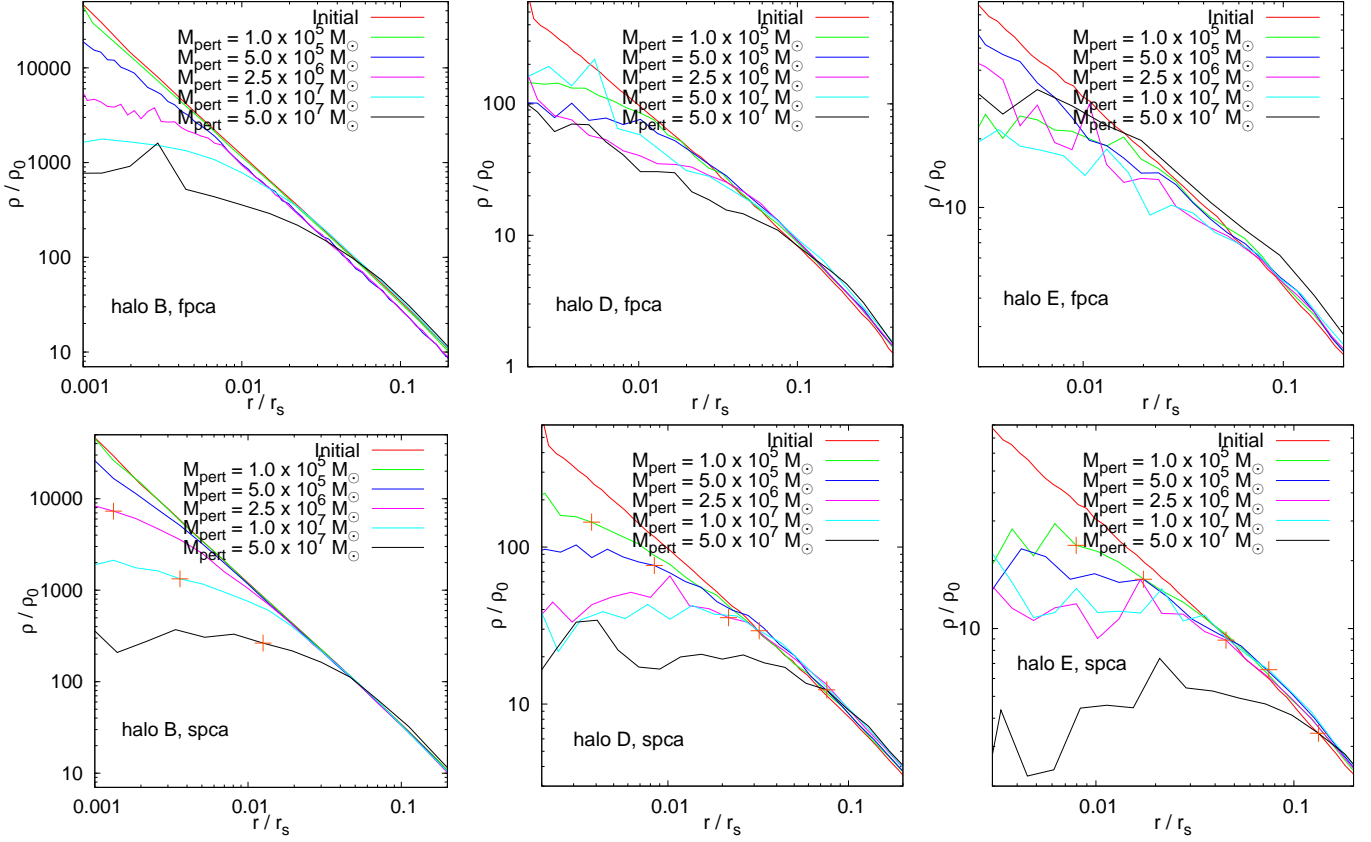


FIG. 4.— Density profiles of the host halo at fpca (upper panel) and spca (lower panel) for the different nuclei masses M_{pert} . From left to right the panels show the haloes B, D and E. Comparing the upper and lower panels, notice that the halo rapidly reaches a new equilibrium – the cored state – between fpca and spca. The orange crosses mark the ‘stalling radii’ where the perturber no longer sinks via dynamical friction. Notice that these lie at the edge of the freshly created core.

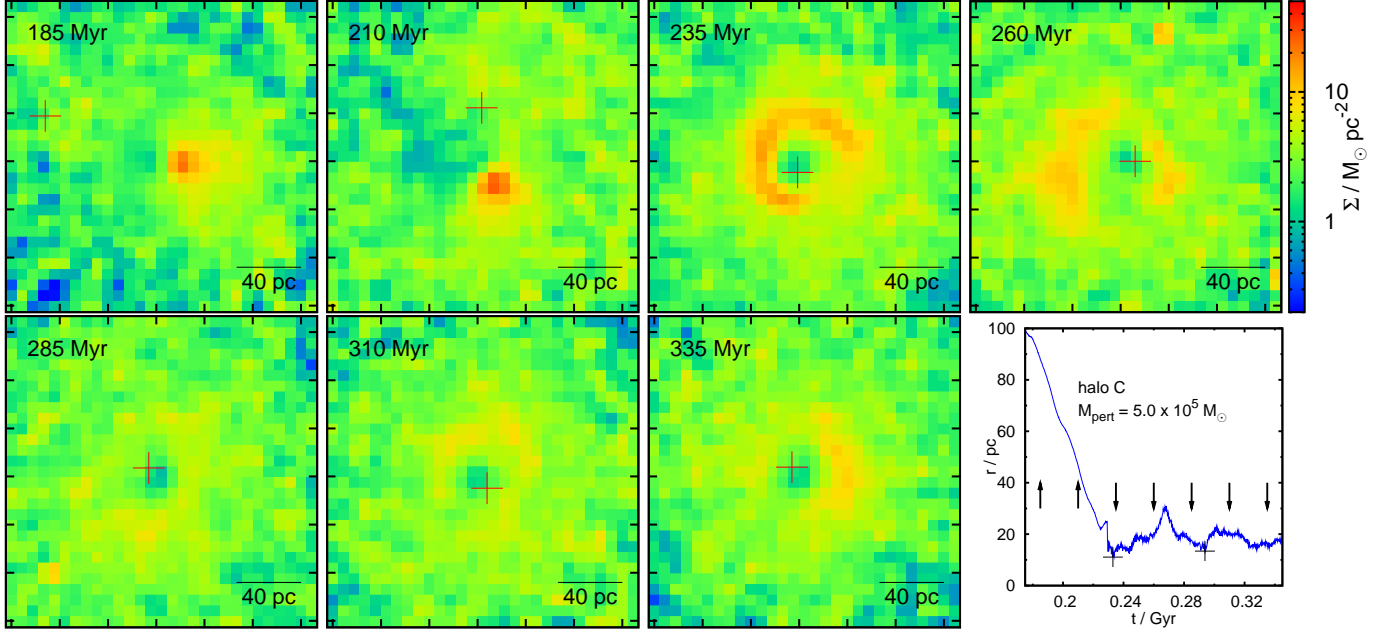


FIG. 5.— 194 pc \times 194 pc density contour maps of background particles within halo C. We select only particles whose orbit lies within the plane of the perturber. The perturber mass was $5 \times 10^5 M_\odot$ and orbits *anticlockwise* on this figure (see red crosses). The different panels show output times: 185 Myr, 210 Myr, 235 Myr (the time of the fpca), 260 Myr, 285 Myr, 310 Myr and 335 Myr. The graph in the lower right corner shows the trajectory from Figure 2. The arrows indicate the above output times and the crosses mark the first and second points of closest approach (fpca and spca).

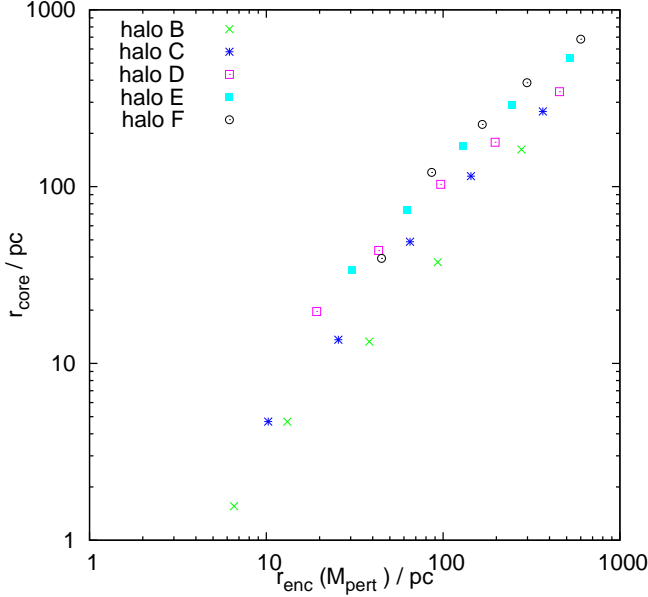


FIG. 6.— The core radius as a function of the radius which encloses the mass of the perturber in the initial conditions. The relation is linear and indicates that the cusp is disrupted to a radius that contains a similar mass as the sinking perturber.

And from equation (1), assuming that $r_t \ll r_s$, this gives:

$$\frac{r_t}{r_s} \sim \left[\frac{(3-\gamma)M_{\text{pert}}}{4\pi\rho_0 r_s^3} \right]^{\frac{1}{3-\gamma}} \quad (5)$$

We can then relate this tidal radius to the core radius via some factor $f(\gamma)$:

$$\frac{r_{\text{core}}}{r_s} = f(\gamma) \left[\frac{(3-\gamma)M_{\text{pert}}}{4\pi\rho_0 r_s^3} \right]^{\frac{1}{3-\gamma}} \quad (6)$$

We find $f(\gamma) = 2 - \gamma$ gives an excellent fit to our simulation results (see Figure 7).

In Figure 8, we show the core radius r_{core} as a function of the initial radius r_i . If tidal shredding is responsible for cusp-core transformations, then there should be no dependence of r_{core} on r_i . This is indeed the case as long as $r_i > r_{\text{core}}$. (Note that since all of the simulations had to be started outside of r_{core} , the very heavy perturbers had to be started further out than the light perturbers.)

Our analytic and numerical results can be compared with previous studies in the literature. El-Zant, Shlosman & Hoffman (2001) use a semi-analytical Monte Carlo approach based on the Chandrasekhar approximation to estimate core sizes. They let 100–500 perturbers, which have a combined mass of 10% of the host halo, sink into a $\gamma = 1.0$ halo. They find $r_{\text{core}} \approx r_s$, where they define r_{core} as the region within which $\rho \approx \rho_0$ is valid. Putting $M_{\text{pert}}/M_{\text{vir}} = 0.1$ into equation (6) we find $r_{\text{core}} = 0.57 r_s$. Goerdt et al. (2008) let 10 live globular clusters, which have a combined mass of 0.28% of the host halo, sink into a $\gamma = 1.0$ halo. They do not measure the core size explicitly, but in their Figure 1 the final dark line becomes very shallow around 50 pc. Putting $M_{\text{pert}}/M_{\text{vir}} = 0.0028$ into equation (6) we find $r_{\text{core}} = 40$ pc. Thus, our estimates agree very well with what has already been published in the literature.

2.2.3. Core-stalling

Once a core is formed, the perturbers stall and do not sink over many dynamical times (see Figure 2). The mechanism for core stalling was discussed in detail in Read et al. (2006a). They suggested that the perturber and background find an equilibrium state where the background moves on epicycles around the perturber, leading to no net momentum transfer. Recently, Inoue (2010) have also found evidence for such a state in their simulations. A prediction of this is that the background has an over-density in the plane of the perturber that lags the motion of the perturber (see Read et al. 2006a, their Figure 4). This can be seen in Figure 5 at late times (recall that the perturber moves in an anticlockwise fashion in this figure).

3. APPLICATIONS

3.1. Dark matter annihilation

The change from cuspy to cored central density is important for the expected annihilation signal from a weakly interactive massive (WIMP) dark matter particle, since the annihilation signal goes as the density squared. The net flux coming from WIMP annihilation is given by (e.g. Koushiappas 2006; Goerdt et al. 2007):

$$F = k \int_{r_{\text{min}}}^{\infty} 4\pi r^2 \rho(r)^2 dr \quad (7)$$

where the dependence of the flux on the WIMP mass and interaction cross section is wrapped up inside the constant k . The lower bound r_{min} is defined as the central region of the host halo in which the neutralinos have already annihilated. The required number density for this to happen can be estimated using:

$$t_h = \frac{1}{n\sigma v} \quad (8)$$

where $t_h \approx 13$ Gyr is the Hubble time, $\sigma v \approx 10^{-30} \text{ cm}^3 \text{ s}^{-1}$ is a typical cross section and n is the number density of neutralinos. For more details see Calcáneo-Roldán & Moore (1999). The minimum radius can now be computed (for a sinking perturber of a given mass) by comparing this minimum number density with the density profile of the lower panel in Figure 4. Assuming a WIMP mass of 100 GeV and deploying the above mentioned density profile, r_{min} is of order 10^{-14} pc. Figure 9 shows the resulting annihilation flux. It is more or less independent of the assumed WIMP mass, because this mass only goes into the calculation of r_{min} , which is very small. For typical core sizes of $r_{\text{core}} \simeq 0.04 r_s$, core creation can lead to a decrease in flux of up to a third. A much weaker effect would result from a single sinking star; for example a $10 M_{\odot}$ star would create a core of radius 0.34 pc in our fiducial halo. However, note that the other core-formation mechanisms discussed in section 1 may play a more important role than the dynamical friction mechanism discussed here. In this case, the annihilation signal could be reduced even further. An increase in the expected signal can also occur if dark matter adiabatically contracts due to gas cooling at the centre of dark matter halos (e.g. Young 1980; Blumenthal et al. 1986). Such astrophysical uncertainties make it currently challenging to predict the expected annihilation signal for a given dark matter model.

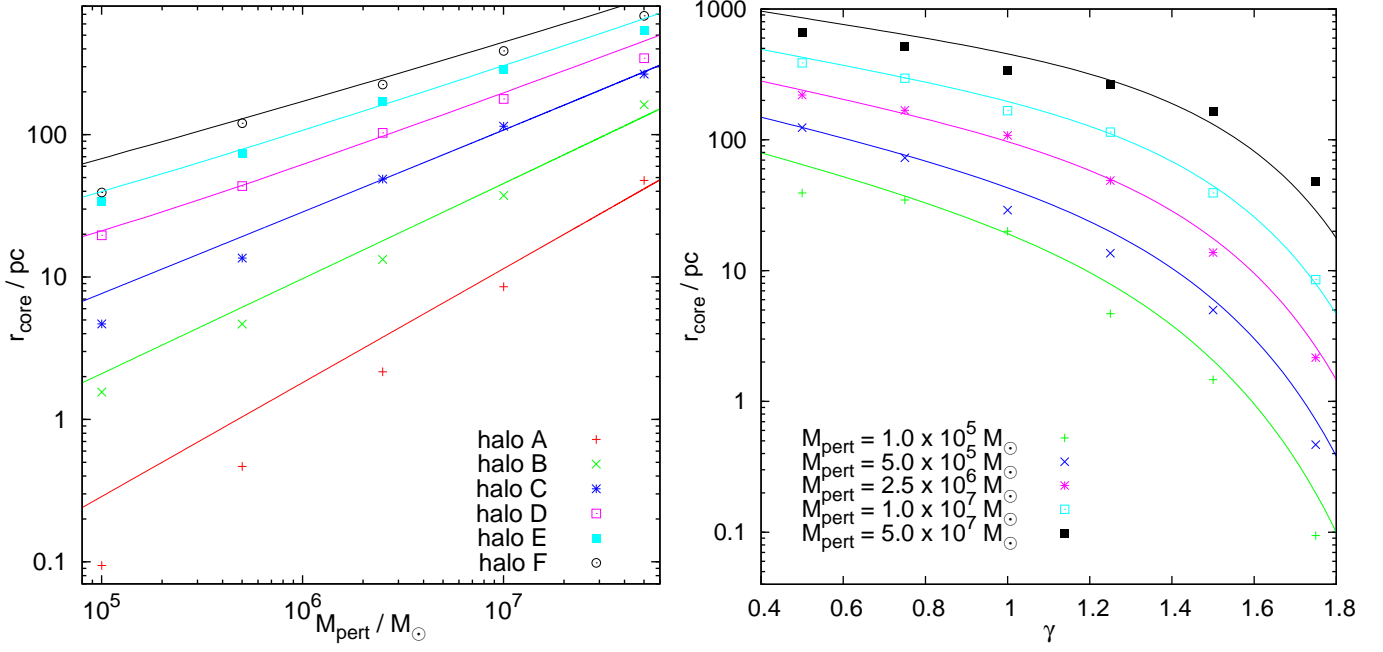


FIG. 7.— The core radii as a function of M_{pert} for different values of γ (left) and as a function of γ for different values of M_{pert} (right). Our model predictions from equation (6) are also shown overlaid (solid lines).

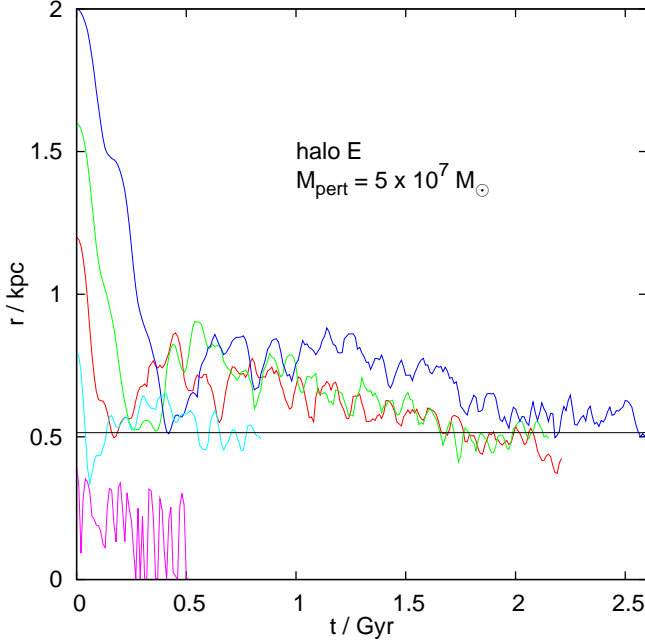


FIG. 8.— Simulated position of a single perturber with identical mass ($5 \times 10^7 M_{\odot}$) but different initial radii within halo E as a function of time. The core radius is indicated by the horizontal black line.

3.2. A new model for close binary nuclei – the ‘stalled binary’ model

There are a number of systems in the universe which show evidence for close binary nuclei (with projected separation $< 100 \text{ pc}$; e.g. Lauer et al. 1993, 1996, 2005; Bender et al. 2005; Houghton et al. 2006; Mast et al. 2006; Debattista et al. 2006). Only three of these are unambiguous binary nuclei systems – M31, NGC 4486B and VCC 128; the rest are more poorly resolved systems that

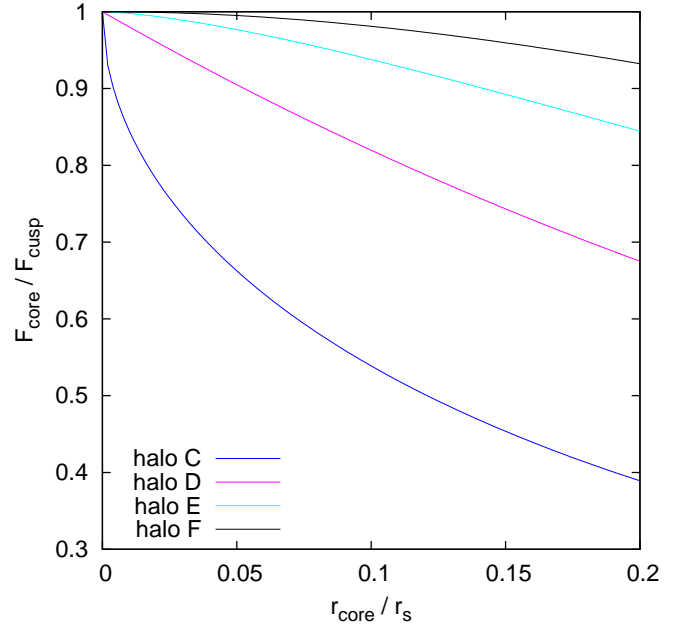


FIG. 9.— The flux of annihilation products from different host haloes after the central cusp core transformation relative to the untransformed initial cusp. Typical core sizes ($r_c \approx 0.04 r_s$) can lead to a decrease in flux of up to one third. Haloes A and B are not shown because the corresponding values for inner log density slopes $\gamma \geq 1.5$ diverge.

show strongly asymmetric central light distributions.

The standard model for these close ‘binaries’ has become the Tremaine (1995) eccentric disc model originally proposed to explain M31 (Lauer et al. 2005). In this scenario, the two central peaks are really an artifact of a central eccentric disc of stars orbiting a black hole. The fainter peak is associated with stars orbiting at pericentre in the disc. The brighter peak is associated with stars

at apocentre where they linger for long times. Key to the success of this model is a near-Keplerian central potential. This ensures that there is no orbital precession so that the bunching at apocentre is maintained over many orbital periods.

For M31, the eccentric disc model works remarkably well since its binary ‘nuclei’ have a projected separation smaller than the sphere of influence of the central black hole (~ 1.8 pc; Peiris & Tremaine 2003; Bender et al. 2005). In addition, more recent observations suggest that the M31 nucleus is really a triple system, where the third nucleus P3 is centred on the central black hole (Bender et al. 2005).

While the eccentric disc model has been a success for M31, it is not clear that it works well for the other ‘close binary’ systems observed to date. Many have significantly larger projected separations than M31 (Lauer et al. 1996, 2005; Debattista et al. 2006), which means that their central potentials may deviate from being pure Keplerian. In addition, both VCC 128 and NGC 4486B have binary nuclei with very similar magnitudes. This requires a tilted ring model, rather than an eccentric disc of stars (Lauer et al. 1996; Debattista et al. 2006), which makes the ‘eccentric disc’ model seem less attractive.

When the double nucleus of M31 was first discovered, Lauer et al. (1993) speculated that the two bright nuclei really were just that – one from M31 and the other the cannibalised centre of a smaller merged galaxy. The primary argument against this was that dynamical friction would cause the nuclei to rapidly coalesce. However, as we have shown here, as binary nuclei sink via dynamical friction, they create a central constant density core. They then stall at the edge of this core experiencing no further friction over many dynamical times. This suggests a new model for the formation of close binary nuclei – the ‘stalled binary’ model.

A particularly interesting candidate system for a ‘stalled binary’ is VCC 128. This has two nuclei that have similar brightness, and a projected separation of ~ 32 pc (Debattista et al. 2006) which presents some tension for the eccentric disc model. As we shall show next, however, the ‘stalled binary’ model works remarkably well. VCC 128 is also especially interesting since it appears to be dark matter dominated at all radii. As a result – if its binary nucleus is a ‘stalled binary’ – VCC 128 gives us a unique opportunity to constrain the central log-slope of the dark matter density profile on very small scales. We consider this special case next.

3.2.1. The binary nuclei in VCC 128

VCC 128 is a dwarf spheroidal galaxy (dSph) at the outskirts of the Virgo cluster with a very close binary nucleus (Debattista et al. 2006). The two nuclei are similar in their appearance with masses estimated to be around $5 \times 10^5 M_\odot$. The projected distance of the two nuclei in VCC 128 is 32 pc. Debattista et al. (2006) suggest, because the two nuclei have very similar colours and magnitudes that this could be evidence for a nuclear disc around a supermassive black hole (SMBH), a situation as in NGC 4486B (Lauer et al. 1996) and similar to the one in M31 (Tremaine 1995). However, it is not confirmed that such an SMBH can exist in a dwarf galaxy like VCC 128. Buyle et al. (2008) do not find

statistically significant evidence for a stellar disk orbiting a central massive black hole from their recent radio continuum observations of VCC 128. Ferrarese (2002) found from a sample of 36 galaxies, tentative evidence that SMBH formation becomes inefficient in haloes below a dynamical mass of $\sim 5 \times 10^{11} M_\odot$, though more recent work may suggest otherwise (Ferrarese et al. 2006; Wehner & Harris 2006). As such, it is interesting to consider whether our new ‘stalled binary’ model can explain VCC 128’s binary nucleus.

The dwarf galaxy VCC 128 is likely dark matter dominated at all radii. We estimate its stellar mass distribution in two different ways. Firstly, we use the Sérsic (1963, 1968) profile parameters derived in Debattista et al. (2006) normalised to give a total luminosity in the B-band of $M_B = -15.5$ mag:

$$\Sigma(R) = \Upsilon_B I_e \exp \left\{ -b_n \left[\left(\frac{R}{R_e} \right)^{\frac{1}{n}} - 1 \right] \right\} \quad (9)$$

with $b_n = 1.9992n - 0.3271$ (Graham & Driver 2005), $n = 0.55$, $R_e = 14.5$ arcsec and assuming a B-band mass to light ratio $\Upsilon_B = 3$ for dE galaxies as in Read & Trentham (2005). We then de-project the stellar mass distribution using the usual Abel integral equation (that assumes spherical symmetry):

$$\rho(r) = -\frac{1}{\pi} \int_r^\infty \frac{d\Sigma(R)}{dR} \frac{dR}{\sqrt{R^2 - r^2}}. \quad (10)$$

The resulting density and cumulative mass distributions are given by the solid lines in Figure 1. Secondly, we use the stellar masses derived from fits to the spectral energy distribution (SED) of the galaxy nucleus and the whole galaxy as given in Debattista et al. (2006). These are overlaid on the right panel of Figure 1 (*crosses*) and give an excellent match to the cumulative mass distribution derived from the Sérsic fit to the light profile. We assume from here on that the dark matter is dynamically dominant and that the stars are to a good approximation a massless tracer population.

Figure 10 shows the time taken for two nuclei that have masses $5 \times 10^5 M_\odot$ and initial separation of 44 pc to sink via dynamical friction in halos B, D, E and F, assuming that equation (2) fully describes the friction process. We chose this initial separation of 44 pc since this is the most likely deprojected distance of the two nuclei (their observed separation on the sky is 32 pc). In all haloes with cusp slopes steeper than 0.75, the nuclei coalesce rapidly. This suggests that, were equation (2) the whole story, it would be very unlikely to observe such a close double nucleus in any dwarf galaxy in Virgo. However, as we have demonstrated in the previous section, the merging nuclei will create a small core and stall indefinitely, leading to a much higher probability of observing double nuclei.

Therefore we ran an additional series of simulations with two perturbers on either coplanar or perpendicular orbits. Again we used the haloes presented in Table 1. The stalling behaviour is shown in Figure 11. In haloes B, D and E, the nuclei do not stall. Only in halo F do they stall above 32 pc. These results suggest for slopes of 1.0 or steeper, this stalling mechanism does not crucially change the results we derived analytically in this section.

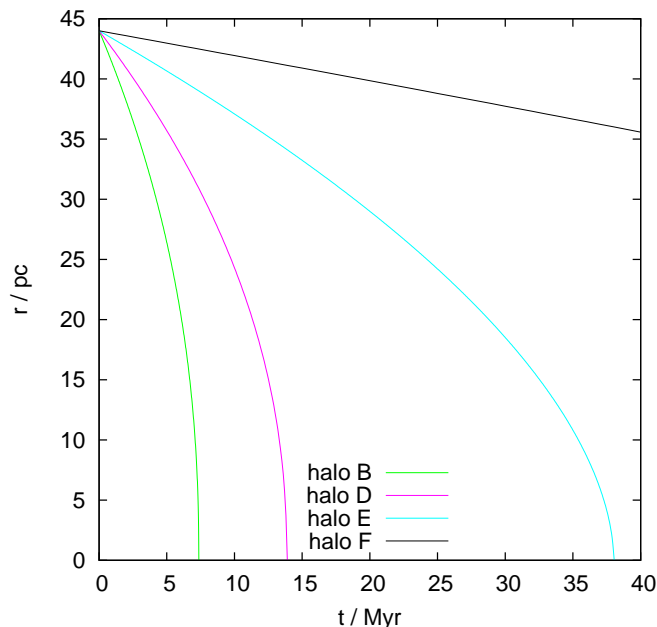


FIG. 10.— Analytical computed position as a function of time, during the Chandrasekhar sink-in period for four of our haloes, assuming an initial true distance of the nucleus from the centre of 44 pc. Haloes A and C are omitted.

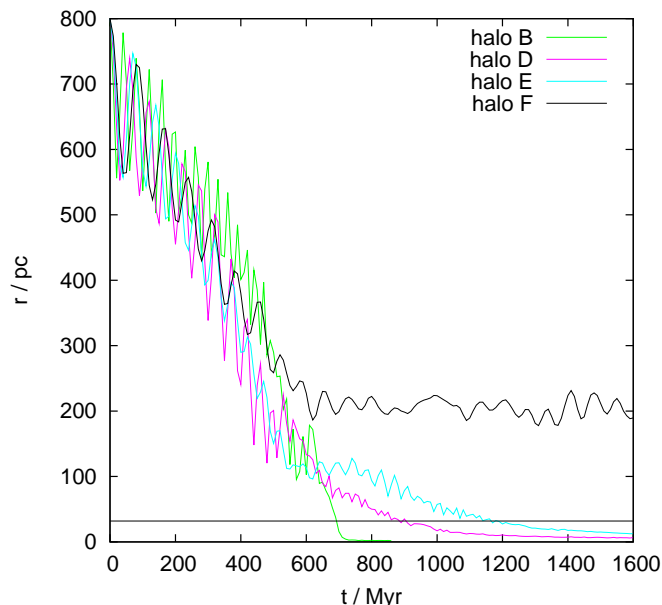


FIG. 11.— Separation of the two perturbers as a function of time, assuming an initial true separation of 800 pc and perpendicular orbits. The horizontal black line shows the observed projected distances in VCC 128. Haloes A and C are omitted.

However for slopes shallower than 1.0 it affects these results quite dramatically. It is interesting that the most recent CDM halo simulations have cusps shallower than 0.7 on these scales (Stadel et al. 2009; Diemand et al. 2008; Springel et al. 2008).

To summarise our findings: assuming that VCC 128 has a core-stalled binary nucleus, we can exclude all steep inner log density slopes of 0.75 or higher. Our current best explanation for VCC 128’s observed binary nucleus is that the two nuclei transformed an initially steeper density profile with an inner log density slope between

0.75 and 0.5 into a core during its initial sinking period. The nuclei then stalled at the edge of this freshly created core. Note that a very shallow inner log density slope like 0.5 is also disfavoured. This is because in this case, the nuclei stall at $\sim 100 - 200$ pc (see Figure 11) creating some tension with the observed projected separation. Therefore we conclude that an underlying dark matter halo with $\gamma \sim 0.5 - 0.75$ at $\sim 1\%$ of the virial radius provides the best explanation for the observations.

One should note here that this cusp-core transformation mechanism does not explain the dynamical friction timescale problem of Fornax within a Λ CDM ($\gamma = 1.0$) halo (see Figure 3 of Goerdt et al. 2006), because in that case the globular clusters in Fornax are too light and too distant from the centre of their host galaxy for this cusp-core transformation mechanism to play a significant role. Equation (6) predicts for Fornax (assuming $\gamma = 1.0$) a core of only 44 pc. This is far smaller than the projected radius of the innermost globular cluster in Fornax, which is at 240 pc.

4. CONCLUSIONS

We have performed a detailed investigation into the disruption of central cusps via the transfer of energy from sinking massive objects. Constant density inner regions form at the radius where the enclosed mass approximately matches the mass of the infalling body. We explored parameter space using numerical simulations and gave an empirical relation for the size of the resulting core within structures that have different initial cusp slopes. We went on to demonstrate that infalling bodies always stall at the edge of these newly formed cores, experiencing no dynamical friction over many dynamical times.

As applications, we considered the resulting decrease in the WIMP annihilation flux due to centrally destroyed cusps; and we presented a new theory for the formation of close binary nuclei – the ‘stalled binary’ model. Our key results are as follows:

1. Core formation due to sinking massive objects can soften a central dark matter cusp reducing the expected WIMP annihilation flux (predicted by structure formation simulations that model dark matter in the absence of baryons) by up to a third.
2. Core formation due to sinking massive objects could help to alleviate the long-standing cusp-core problem (see eg: Spekkens, Giovanelli & Haynes 2005; Moore 1994; de Blok, McGaugh & Rubin 2001). From equation (6), a ~ 1 kpc sized core will form from perturber having $\sim 1\%$ of the mass of the host. This recovers the earlier results of El-Zant, Shlosman & Hoffman (2001) and Jardel & Sellwood (2009). However, such massive infalling perturbers must later disrupt or be removed in order to be consistent with the low surface density of stars and gas observed in galaxies where the cusp-core problem is most apparent.
3. Infalling nuclei at the centres of galaxies will evacuate a core and stall indefinitely, provided that the initial background density is not significantly steeper than r^{-1} . This could explain a number of binary nuclei systems in the Universe.

4. We focused on the special binary nucleus system VCC 128 since it is dark matter dominated at all radii. Assuming that its binary nucleus can be explained by our ‘stalled binary’ model, we found that the initial inner log density slope γ of the dark matter halo of VCC 128 must be $0.5 < \gamma < 0.75$ at $\sim 0.1\%$ of the virial radius. For $\gamma > 0.75$ initially, the dynamical friction sink-in time is so small in comparison to the lifetime of the galaxy that we run into a fine tuning problem. For $\gamma < 0.5$ initially, the nuclei stall far beyond their current projected separation of 32 pc. For $0.5 < \gamma < 0.75$ initially, the nuclei create a central constant density core of separation ~ 40 pc after which they stall

indefinitely. Our preferred inner slopes are consistent with those found in the recent billion particle CDM halo simulations of Stadel et al. (2009), Diemand et al. (2008) and Springel et al. (2008).

It is a pleasure to thank Ioannis Sideris and Eyal Neistein for carefully reading the manuscript. For all N -body simulations we used PKDGRAV2 (Stadel 2001), a multi-stepping tree code developed by Joachim Stadel. All computations were made on the zBox2 supercomputer at the University of Zürich. Special thanks go to Doug Potter for bringing it to life. Tobias Goerdt is a Minerva fellow.

REFERENCES

- Beers T. C, Tonry J. L, 1986, ApJ, 300, 557
 Bender R. et al, 2005, ApJ, 631, 280
 Blumenthal G. R, Faber S. M, Flores R, Primack J. R, 1986, ApJ, 301, 27
 Boylan-Kolchin, M., Ma C., Quataert, E., 2004, ApJ, 613, L37-L40
 Buyle P, de Rijcke S, Debattista V. P, Ferreras I, Pasquali A, Seth A, Morelli L, 2008, ApJ, 685, 915
 Calcáneo-Roldán C, Moore B, 2000, Phys. Rev. D, 62, 123005
 Capuzzo-Dolcetta R, Vicari A, 2005, MNRAS, 356, 899
 Chandrasekhar S, 1943, ApJ, 97, 255
 Colpi M, Mayer L, Governato F, 1999, ApJ, 525, 720
 Debattista V. P, Ferreras I, Pasquali A, Seth A, de Rijcke S, Morelli L, 2006, ApJ, 651, 97
 de Blok W. J. G, McGaugh S. S, Rubin V. C, 2001, AJ, 122, 2396
 de Rijcke S, Michielsen D, Dejonghe H, Zeilinger W. W, Hau G. K. T, 2005, A&A, 438, 491
 Diemand J, Moore B, Stadel J, 2005, Nature, 433, 389
 Diemand J, Kuhlen M, Madau P, Zemp M, Moore B, Potter D, Stadel J, 2008, Natur, 454, 735
 Dubinski J, Carlberg R. G, 1991, ApJ, 378, 496
 El-Zant A, Hoffman Y, Primack J, Combes F, Shlosman I, 2004, ApJ, 607, 75
 El-Zant A, Shlosman I, Hoffman Y, 2001, ApJ 560, 636
 Ferrarese L, 2002, ApJ, 578, 90
 Ferrarese L, Côté P, Dalla Bontà E. et al, 2006, ApJL, 644, 21
 Goerdt T, Gnedin O. Y, Moore B, Diemand J, Stadel J, 2007, MNRAS, 375, 191
 Goerdt T, Moore B, Kazantzidis S, Kaufmann T, Macciò A. V, Stadel J, 2008, MNRAS, 385, 2136
 Goerdt T, Moore B, Read J. I, Stadel J, Zemp M, 2006, MNRAS, 368, 1073
 Graham A. W, Driver S. P, 2005, PASA, 22, 118
 Gualandris A, Merritt D, 2008, ApJ, 678, 780
 Gunn J. E, Lee B. W, Lerche I, Schramm D. N, Steigman G, 1978, ApJ, 223, 1015
 Hernquist L, 1990, ApJ, 356, 359
 Hernquist L, Weinberg M. D, 1989, MNRAS, 238, 407
 Houghton R. C. W, Magorrian J, Sarzi M, Thatte N, Davies R.L, Krajnović D, 2006, MNRAS, 367, 2
 Inoue S, 2009, MNRAS, 397, 709
 Inoue S, 2010, arXiv:0912.2409
 Jandel J. R, Sellwood J. A, 2009, ApJ, 691, 1300
 Kalnajs, A. J, 1972, in Lecar M, ed, Proc. IAU Colloq. 10, Gravitational N -Body Problem, Reidel, Dordrecht
 Kazantzidis S, Magorrian J, Moore B, 2004, ApJ, 601, 37
 King I. R, 1966, AJ, 71, 64
 Kleya J. T, Wilkinson M. I, Gilmore G, Evans N. W, 2003, ApJ, 588, 21, Erratum-ibid, 2003, 589, 59
 Koushiappas S. M, 2006, Phys. Rev. Lett, 97, 191301
 Lake G, 1990, Nature, 346, 39
 Lauer T. R. et al, 1993, AJ, 106, 1436
 Lauer T. R. et al, 1996, ApJ, 471, 79
 Lauer T. R. et al, 2005, AJ, 129, 2138
 Lin D. N. C, Tremaine S, 1983, ApJ, 264, 364
 Lokas E. L, 2002, MNRAS, 333, 697
 Ma C, Boylan-Kolchin M, 2004, PhRvL, 93, 021301
 Mast D, Díaz R. J, Agüero M. P, 2006, AJ, 131, 1394
 Merritt D, Piatek S, Portegies Zwart S, Hemsendorf M, 2004, ApJL, 608, 25
 Michie R. W, 1963, MNRAS, 125, 127
 Michie R. W, Bodenheimer P. H, 1963, MNRAS, 126, 269
 Milosavljević M, Merritt D, Rest A, van den Bosch F. C, 2002, MNRAS, 331, 51
 Moore B, 1994, Nature, 370, 629
 Navarro J. F, Frenk C. S, White S. D. M, 1996a, ApJ, 462, 563
 Navarro J. F, Eke V. R, Frenk C. S, 1996b, MNRAS, 283, L72
 Peiris H. V, Tremaine S, 2003, ApJ, 599, 237
 Power C, Navarro J. F, Jenkins A, Frenk C. S, White S. D. M, Springel V, Stadel J, Quinn T, 2003, MNRAS, 338, 14
 Read J. I, Gilmore G, 2005, MNRAS, 356, 107
 Read J. I, Goerdt T, Moore B, Pontzen A. P, Stadel J, Lake G, 2006a, MNRAS, 373, 1451
 Read J. I, Wilkinson M. I, Evans N. W, Gilmore G, Kleya J. T, 2006b, MNRAS, 366, 429
 Read J. I, Trentham N, 2005, RSPTA, 363, 2693
 Romano-Díaz E, Shlosman I, Hoffman Y, Heller C, 2008, ApJ, 685, L105
 Saha P, 1992, MNRAS, 254, 132
 Sellwood J. A, 2006, ApJ, 637, 567
 Sánchez-Salcedo F. J, Reyes-Iturbide J, Hernandez X, 2006, MNRAS, 370, 1829
 Sérsic J. L, 1963, BAAA, 6, 41
 Sérsic J. L, 1968, Atlas de galaxias australes
 Silk J, Bloeman H, 1987, ApJ, 313, L47
 Spekkens K, Giovanelli R, Haynes M. P, 2005, AJ, 129, 2119
 Springel V, Wang J, Vogelsberger M. et al, 2008, MNRAS, 391, 1685
 Stadel J, 2001, PhD thesis, Univ. Washington
 Stadel J, Potter D, Moore B. et al, 2009, MNRAS, 398, 21
 Tonini C, Lapi A, Salucci P, 2006, ApJ, 649, 591
 Tremaine S, 1995, AJ, 110, 628
 Tremaine S, Weinberg M. D, 1984, MNRAS, 209, 729
 Wehner E. H, Harris W. E, 2006, ApJL, 644, 17
 White S. D. M, 1983, ApJ, 274, 53
 Young P, 1980, ApJ, 242, 1232
 Zemp M, Moore B, Stadel J, Carollo C. M, Madau P, 2008, MNRAS, 386, 1543
 Zhao H, 1996, MNRAS, 278, 488